THAMYRES FERNANDES MESSA MOREIRA

The Nanoscale Designing of Electrodes Aimingat the Development of High-PerformanceSupercapacitors

Relatório de Pós-doutorado realizado na Universidade Estadual Paulista (UNESP), Instituto de Quimica, Departamento de Engenharia, Física e Matemática , Araraquara-SP.

Supervisor(a): Prof. Dr. Paulo Roberto Bueno

Fundação de Amparo à Pesquisa do Estado de São Paulo FAPESP - 2021/00726-8

Araraquara-SP

2024

Resume: Throughout this project, we utilized the Quantum Rate Spectroscopy (QRS) technique to examine the electronic structure of graphene-derived nanofilms in a 2D configuration at room temperature. This method allowed us to avoid the complexity of vacuum conditions, making it both efficient and cost-effective. Our research centered on the supercapacitance phenomena in reduced graphene oxide structures from a quantum mechanical rate theory perspective. While traditional views primarily link supercapacitance in carbon materials to electrostatic capacitance, which depends on surface area, our findings reveal that quantum rate theory introduces an overlap between electrostatic and chemical (quantum) capacitance states. This discovery provides a more detailed understanding of the energy dynamics within these materials.

In exploring these quantum capacitance states, we uncovered an energy overlap between the electrostatic and quantum capacitive energy levels in reduced graphene oxide. Our results show that the charge dynamics in these structures adhere to a quantum resistance limit, consistent with quantum electrodynamics principles. This research sheds light on a new aspect of electron behavior in nanoscale carbon structures, offering significant insights into the unique properties of graphene-based materials and their potential applications in energy storage.

Building on the foundational understanding gained from our studies of 2D nanostructures, we advanced to the development of 3D symmetric supercapacitors. This was achieved by incorporating functional groups and redox-active molecules, such as p-phenylenediamine (PPD), to modify graphene derivatives, enhancing their suitability as symmetric electrodes in supercapacitor devices.

The achievements of this project are substantial, highlighted by the submission of a paper titled The Quantum Mechanical Origin of the Supercapacitance Phenomenon in Reduced Graphene Oxide Structures to the Carbon journal. Additionally, five other papers are nearing completion, further emphasizing the importance of this work.

1 Developed activities and productivity

During this period, we employed the Quantum Rate Spectroscopy (QRS) technique to investigate the electronic structure of graphene-derived nanofilms (2D configuration) at ambient temperature, thereby eliminating the need for vacuum conditions, which turns this spectroscopic method into a simple and low-cost methodology. We investigated supercapacitance phenomena observed in reduced graphene oxide structures from a quantum mechanical rate viewpoint. The supercapacitance phenomenon in carbonaceous materials has been majorly attributed to electrostatic capacitance contributions, in which the magnitude of this capacitance is correlated with the amount of surface area available to be charged under the presence of electric potential perturbations. Nonetheless, the quantum rate theory predicts a superposition between electrostatic C_e and chemical C_q (also called quantum) capacitance energetic levels. The superposition of these capacitive states implies that the electric potential perturbation not only drives the separation of charges in space (thus correlating with the geometry of the capacitor and consequently with the surface area) but also governs the occupancy of the electric-field screened electronic structure of reduced graphene oxide embedded in the electrolyte environment. This leads to an energy degeneracy between electrostatic e^2/C_q and quantum e^2/C_q capacitive energy states, as confirmed in this work for reduced graphene oxide carbonaceous structures. Accordingly, the analysis proves that the charge dynamics associated with the resistance for charging the pseudo-capacitive $E = e^2/C_q$ states of reduced graphene oxide structure follows a quantum resistance limit $R_K = h/e^2 \sim 25.8$ kΩ within a charging frequency of $\nu = 1/R_K C_q = E/h = e^2/hC_q$ that obeys quantum electrodynamics principles, in agreement with the premises of the quantum rate theory. Two energy levels associated with the occupancy of the electronic states upon the reduction of graphene oxide were identified. These results illuminate a new phenomenology of electron dynamics in nanoscale carbonaceous structures. This research contributes to an enhanced understanding of the distinctive properties of nanoscale graphene-based materials, holding potential implications for the advancement of energy storage technologies. Following the initial characterization of 2D nanostructures, we have successfully developed exceptional 3D symmetric supercapacitors. This achievement was realized through the incorporation of functional groups and redox molecules, such as p-phenylenediamine (PPD), to modify graphene derivatives for use as symmetric electrodes in supercapacitor devices. Derived from the progress made during the postdoctoral project, we already submitted a paper entitled *The Quantum Mechanical Origin of the Supercapacitance Phenomenon in Reduced Graphene Oxide Structures* to carbon journal from Elsevier publisher. At the same time, all experimental data was gathered and processed, and the other five papers are now in the final stages of writing and revision.

1 *1-Understanding the rGO electronic density using a easy and low cost spectroscopic tool*

Brief: In this study we are proposing the scrutiny of the DOS rGO based materials in order to understand the relation between the DOS and the supercapacitance behavior of GQDs.

2-Enhancing the Electronic Characterization of Graphene Quantum Dots by Quantum Rate Spectroscopy

Brief: In this study, we are discussing and exploring the energy storage mechanism for this graphene derivated to better understand the relation between the DOS and the supercapacitance behavior of GQDs.

3-Electroactive Electrolytes: A Breakthrough in Supercapacitor Development for Sustainable Energy Storage

Brief: In this study, we are investigating the effects of electroactive electrolytes in the supercapacitor's energy storage mechanism in the electrochemical double-layer capacitors.

4-Electrochemical and Electronic Characterization of Perovskite-Like Composites from Quantum Rate Spectroscopy

Brief: For this publication, we are analyzing the density of states (DOS) for perovskite-like composites in different compositions to gain a deeper understanding of the energy impact of the metals effects in the composite's DOS.

5- Design and Characterization of a Cobalt-Based anode electrode for Enhanced Performance in Asymmetric Supercapacitors

Brief: We aim to present in the literature the outstanding results (approximately 350 Fg^{-1}) achieved through the optimization of the ratio between hexacyanocobalt ferrate complexes and reduced graphene oxide for highly efficient anodes in supercapacitor devices.

1.1 Introduction

Ongoing efforts to design energy storage devices with high energy densities and rapid charging capabilities have intensified the search for chemical structures and electrochemical interfaces that demonstrate supercapacitive properties [1, 2]. From a fundamental perspective, the supercapacitance phenomenon has been attributed to electrostatic effects, such as in the case of electrical double-layer based supercapacitors, or to pseudocapacitive effects, as observed in nanostructured transition metal oxide [3, 4, 5, 6, 7, 8, 9, 10].

Carbonaceous materials, notably reduced graphene oxide (rGO), have emerged as promising candidates for supercapacitor applications, owing to their exceptional electrical conductivity, superior mechanical strength, and scalability for industrial production. Nevertheless, although the supercapacitive feature of rGO structures has been extensively characterized by electrical approaches, such as cyclic voltammetry (CV) [11, 12], in-depth studies exploring the origin and physical nature of this phenomenon are scarce and inconclusive. This scenario highlights a gap in our understanding of this electrical phenomenon that requires additional research to reveal the origins of the supercapacitance of rGO structures, which will be conducted here by using time-dependent electrical methods. For instance, these methods have proven to be effective in providing quantum

mechanical insights into various nanoscale structures comprising semiconductors [13, 14] and graphene [15, 16].

Over the past few years, progress has been made in understanding diffusionless electrochemical reactions within redox self-assembled modified interfaces, primarily through time-dependent electrochemical impedance measurements [17]. Alarcon et al. [18], for instance, introduced a straightforward methodology aimed at calculating the electron transfer (ET) rate constant of diffusionless electrochemical reactions that relied on determining the quantum capacitance C_q response of the interface either derived from CV curves or impedance-derived capacitance spectroscopic methods.

Impedance-derived capacitance spectroscopy allows the measurement of the quantum conductance G associated with the ET reaction, permitting to demonstrate of the correlation [19] existing between $G = 1/R_q$ and the quantum capacitance C_q, in such a way that the frequency ν associated with the ET rate constant, demonstrated to be $\nu = 1/R_qC_q$ [18, 20], where measured $R_q = 1/G_0$ was in close agreement to the theoretical value of resistance quantum $h/g_se^2 \sim 12.9$ kΩ, where e is the elementary charge of the electron, h is the Planck constant and $g_s = 2$ is the spin degeneracy of the electron. The demonstration that the charge transfer resistance of diffusionless electrochemical reactions is $R_q = h/g_se^2$ enhanced our understanding of chemical reactions driven by electrons, not only by revealing the quantum nature of the electrochemical reactions but also by permitting us to quantify and measure the quantum electrodynamics of these reactions.

The above-introduced quantum mechanical analysis of ET permitted us to conclude that the ET rate dynamics of diffusionless electrochemical reactions obey quantum electrodynamics that follows Planck-Einsteifn's $E = h\nu$ relationship [21, 17], where $E = e^2/C_q$ is the energy associated with the reaction, in which the ET rate constant is accounted as $\nu \propto e^2/hC_q$, being solely a function of C_q, which is experimentally accessible by CV or impedance-derived capacitance spectroscopic methods. As the rate $\nu \propto e^2/hC_q$ is solely a function of the quantum mechanical experimentally measured C_q parameter, this rate is referred to as quantum rate and the fundamental theory associated with it is referred to as quantum-rate theory [22, 17].

Following $E = h\nu$ quantum electrodynamics phenomenology, it has been [14, 23] demonstrated the viability of employing time-dependent perturbations of modified electrodes containing accessible quantum states to measure the electronic structure of the electrode's interface. The assessment of the electronic structure is possible owing to the measurable C_q being proportional to the density-of-states (DOS), corresponding to the number of states dn per interval of energy dE, such as the DOS is (dn/dE), in which associated energy state $E = e^2/C_q$ levels can be quantified. This spectroscopic method has been referred to as quantum-rate spectroscopy (QRS) and was useful in measuring the electronic structure of cadmium telluride (CdTe) quantum dots (QDs) [14], in which the measured spectrum was in good agreement with that obtained by scanning tunneling spectroscopy (STS). The advantage of QRS over STS is that QRS allows to measure the electronic structure of CdTe QDs at room temperature and electrolyte environment, whereas STS requires ultra-high vacuum and low-temperature conditions.

Equivalent and additionally to CdTe QDs, QRS was applied to measure the elec-

tronic structure of graphene [23] in good agreement with angle-resolved photoemission spectroscopy (ARPES), in which it was demonstrated that the electronic structure of graphene is possible to be measured at room-temperature and electrolyte environment by employing an inexpensive hand-held electrochemical piece of equipment instead of the expensive infrastructure required in the case of using ARPES. Finally, QRS was also successfully employed to characterize the electronic structure and the density-of-states (DOS) of Cu_2O/CuO mixed valence nanoscale films [13].

1.1.1 Quantum Rate Spectroscopic Principles

The possibility of using the quantum electrodynamics principles within the QR theory as a spectroscopic tool at room temperature and electrolyte environment is quite suitable for investigating the electronic structure of low-dimensional materials (such as zero [14], one- [18] and two-dimensional [16] structures [14, 13, 23]) using time-dependent electrochemical methods such as QRS.

The methodology within the QRS approach is quite simple. It consists of applying a time-dependent potential perturbation $V(t) = \bar{V} + \tilde{V}$ in the electrode's interface and measuring the electric current response $i(t) = \bar{i} + \tilde{i}$, where the bar represents the steady-state bias potential $\bar{V}$ or DC electric current $\bar{i}$ at steady-state and the tilde is a time-dependent potential modulation $\tilde{V}$ over a steady-steady potential $\bar{V}$ with an electric current response of $\tilde{i}$. The potential perturbation $\tilde{V}$ within an electric current response $\tilde{i}$ over the steady-state potential $\bar{V}$ of the electrode can be mathematically expressed as $\exp(j\omega t) = \cos(\omega t) + j\sin(\omega t)$, where $j = \sqrt{-1}$. The amplitude of the potential signal is denoted as $|V_0|$ whereas the amplitude of the electric current response is $|I_0|$. The ratio between the time-potential perturbation $V(t)$ and time-dependent current response $i(t)$ is a type of electric transfer function that permits a spectroscopic analysis for which the complex admittance of the signal is $G^*(\omega) = \tilde{i}/\tilde{V} = j\omega C^*(\omega)$ with its inverse being known as impedance, denoted as $Z^*(\omega) = \tilde{V}/\tilde{I} = 1/[j\omega C^*(\omega)]$, constituting a particular complex electric transfer-function of the interface. From the aforementioned admittance or impedance functions, a particular complex $C^*(\omega)$ capacitance spectrum [24], corresponding to the response of a single resistance-capacitance (RC) relaxation process, can be obtained as

$$C^*(\omega) = \frac{C_{q,0}}{1 + j\omega\tau} \sim C_{q,0}\,(1 - j\omega\tau) + O(\omega^2), \tag{1.1}$$

where $C_{q,0}$ is the low-frequency response of the spectrum (obtained for $\omega \to 0$), constituting the quantum capacitance of the electrode's interface modified with low-dimensional structures. Note that $\tau = R_q C_q$ corresponds to the characteristic time constant associated with the quantum rate $\nu = 1/\tau \propto e^2/hC_q$ [16, 23] electrodynamics within the interface.

The main purpose of the present work is to demonstrate that the quantum mechanical meaning of the pseudocapacitance of rGO upon the reduction of the GO, which will be conducted using the QR spectroscopic approach, follows the QR electrodynamics principles. The resulting capacitance spectra upon the electrochemical reduction of GO to

rGO are thus interpreted according to Eq. 1.2 using both equivalent circuit analysis and QRS principles combined. The analysis will be carried out separately on GO and rGO assembled over a cysteamine modified-gold electrode in which a self-assembled monolayer (SAM) of cysteamine is used as a molecular bridge for the anchoring of GO/rGO over the electrode permitting to access the reduced DOS of GO component of the film by measuring the C_q states of the interface separately from the classical polarization (dielectric relaxation).

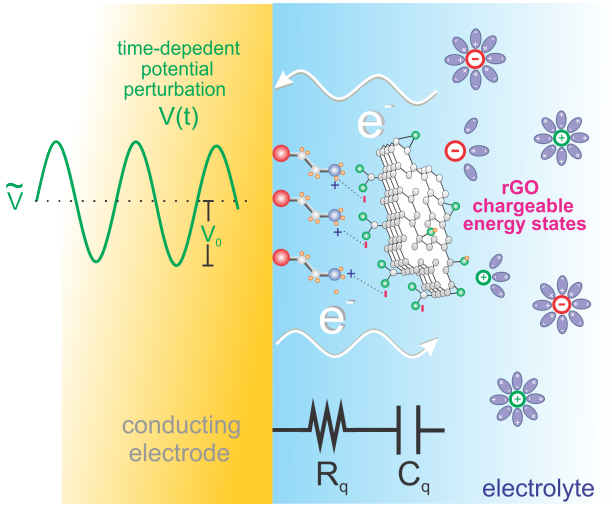

Figura 1.1: Graphic representation of a quantum point contact junction, where a quantum point or nanoscale entity is electronically coupled to a conducting electrode through a quantum bridge. A time-dependent electrical perturbation is applied over this junction enabling the electron communication between the electrode states and the quantum point states, which from the perspective of QRT can be modeled by quantum resistance (R)-capacitance (C) dynamics. Within this dynamics, the electrical field screening process, performed by the ions of the electrolyte medium, is key for access to the quantum insights of the junction. This screening leads to the formation of a quantum electrochemical dipole, which in turn ensures the overlapping of the capacitive states of the interface ($C_e = C_q$).

$$C^*(\omega) = \frac{C_q}{1 + j\omega\tau} \sim C_q\,(1 - j\omega\tau) + O(\omega^2), \tag{1.2}$$

2 Experimental Section

2.1 2D ELECTRODES CARACTERIZATION

2.1.1 Au-Cys, Au-Cys-GO, and Au-Cys-rGO Film Assemblies

Following literature procedures [25], polycrystalline gold surfaces (2 mm diameter gold electrodes from METROHM) were coated with cys-SAM after the mechanical polishment of the surface with alumina suspensions of different sizes (1, 0.3, and 0.05 μm). After the mechanical polishment, the electrodes were electrochemically cleaned using cyclic voltammetry (CV) under basic conditions (0.5 mol L^{-1} NaOH, in which the potential window used was from 1.7 to 0.5 V) and acidic conditions (0.5 mol L^{-1} H_2SO_4, in which the potential windows used was from 0.2 to 1.5 V) at a scanning rate of 100 mV s^{-1} for 200 and 50 cycles, respectively.

The acid condition was maintained until reproducible CVs were associated with oxidation and reduction of the gold surface. After the thorough washing of the surface of the gold electrode with deionized water was performed aiming at removing any physisorbant.Subsequently, the electroactive area of the gold electrode was determined by integrating the cathodic peak obtained for the gold electropolishing CV-based process, using a conversion factor of 410 μC cm^{-1} [26, 27, 28]. The electroactive area was used to normalize the values of electric current (to obtain the current density) and capacitance (capacitance values were normalized in this work per unit of electroactive area of the gold electrode).

To fabricate Au-cys-SAMs interfaces, the polished and cleaned gold electrode surfaces were immersed in a 20 mmol L^{-1} aqueous solution containing cystamine·2HCl for 16 h and then washed thoroughly with Milli-Q ultrapure water to remove any physisorbant. The gold-modified electrode with cys-SAM was immersed in a GO suspension (2 mg mL^{-1}, pH 3.0) for 4 h, during which the positively charged cys-SAM permits the formation of GO layer over it with a predicted thickness between 1.2 to 2 nm [25].

After washing the electrode (Au-cys-SAM-GO) with Milli-Q ultrapure water, electrochemical measurements were performed. [25] experimentally observed that the thickness of the rGO film remained unchanged (between 1.2 to 2 nm) after the electrochemical reduction of GO. Specifically, to carry out the reduction of Au-cys-SAM-GO to Au-cys-SAM-rGO, CV analysis was performed at a scan rate of 10 mV s^{-1} in 0.1 mol L^{-1} KNO_3 aqueous solution within a potential window in between 0.0 to -1.2 V (*versus* Ag/AgCl, 3 mol L^{-1}) for 2 cycles.

2.1.2 Electrochemical Measurements

CV and impedance measurements of the interface were carried out using a portable potentiostat (PalmSens4) equipped with a frequency response analyzer (FRA) in a three-electrode configuration and controlled by PSTrace 5.9 software. Ag|AgCl (3 M KCl) and platinum mesh served as reference and counter electrodes, respectively. The time-dependent impedance spectroscopic method was conducted for frequencies ranging from 1 MHz down to 10 mHz with an amplitude of 10 mV (peak to peak) acquired at the OCP (open-circuit potential) of the electrode. The complex capacitance function $C^*(\omega) = C' + jC''$ (ω is the angular frequency) is of particular importance within the quantum rate theory, as discussed in the context of Eq. 1.2. The complex capacitance function is obtained from impedance measurements of the interface, permitting to obtain the complex capacitance $C^*(\omega) = C' + jC''$ from the complex impedance $Z^*(\omega) = Z' + jZ''$ function from where $C^*(\omega) = 1/j\omega Z^*(\omega)$ is obtained and in which $j = \sqrt{-1}$. The real $C' = \varphi Z''$ and imaginary $C'' = \varphi Z'$ components of $C^*(\omega)$ are hence directly calculated from the measurable $Z^*(\omega) = Z' + jZ''$, where $\varphi = 1/\omega|Z|^2$ and $|Z|$ is the modulus of the impedance.

2.1.3 Raman Spectroscopic Analysis

Raman spectroscopy was employed as a structural spectroscopic method to validate the configuration of the assemblies and characterize the formation of rGO from GO. Raman spectra of the films were obtained using a Micro Raman spectrometer (LabRAM HR, Horiba Jobin Yvon) equipped with an optical microscope to perform Raman measurements with a spatial resolution of 1 μm 2 (objective lens of 50×). The spectral range that was analyzed ranged from 1200 to 3000 cm^{-1}, meanwhile, a 29 mW HE-Ne laser (632.8 nm, 1.96 eV) was utilized.

2.2 3D Graphene-based nanocomposites electrodes preparation

In the initial stage, a nanocomposite ink comprising rGO-PPD and activated carbon was meticulously formulated by blending the composite in precise mass proportions: 15 wt% rGO-PPD, 80 wt% activated carbon, and 5 wt% polyvinylidene fluoride (PVDF). This resulting composite was then homogeneously dispersed in a suitable quantity of N-methyl-2-pyrrolidone (NMP) as the solvent. The formulated ink was subsequently applied to 316 stainless steel current collectors (0.5 mm thickness, 15.8 mm diameter) and allowed to undergo a controlled drying process overnight at 70°C. Following the drying phase, the electrodes were meticulously assembled into coin-cell CR2032-type cells, in a symmetric configuration utilizing an appropriate separator for both aqueous and acetonitrile mediums. The electrolyte was then introduced into the assembled cells. The finalized symmetric assembly was hermetically sealed using a manual hydraulic press.

2.2.1 3D electrodes electrochemical characterization

The fabricated coin-cell symmetric supercapacitor was tested in an operated potential of 2 V. The energy density and power density of the symmetric supercapacitor were determined from the charge-discharge experiments and calculated. Where, the $E_{(cell)}$ is energy density of the cell in Wh kg^{-1}, $C_{(cell)}$ is specific capacitance in F g^{-1}) and $P_{(cell)}$ is power density W kg^{-1}.

3 Results and Discussion

The amine groups of the formed Au-cys-SAM interface were protonated at a pH of 2.5 and pKa of 7.6 following procedures reported in the literature [29] for positively charging the amine groups in the cys-SAM structure. These positively charged centers are susceptible to electrostatic interaction with negatively charged GO platelets, conducting the attachment of graphene oxide platelets on the cys-SAM surface with suitable control of the thickness as noted in reference [30]. As a result, this electrostatic self-assembly procedure allowed us to prepare GO films by modifying Au-cys-SAM structures, permitting the subsequent electrochemical reduction of the GO component of Au-cys-SAM-GO films.

The purpose of reducing the GO electrochemically is to have better control of the electronic defects formed on the GO attached to the electrode via the cys-SAM bridge. As previously noted, the supercapacitance of rGO is fundamentally dependent on the degree of reduction of GO [31, 32, 33], which cannot be exclusively associated with the surface area owing to the superposition of geometric/electrostatic C_e and chemical/quantum C_q capacitance, as predicted by the QR theory. To confirm this prediction of the theory, the controllable electrochemical reduction of the GO in the interface is desirable to track the modification of the electronic structure upon the measurement of the capacitance of the interface using Eq. 1.2, where the interfaces were analyzed using the quantum RC circuit viewpoint within Eq. 1.2.

Before presenting details of this quantum mechanical RC circuit analysis of the interface, the structural and electrochemical characterization of the Au-cys-SAM-rGO films using Raman spectroscopy and CV will be presented.

3.1 Raman Spectroscopy and Cyclic Voltammetry

The modification of cys-SAM with GO established through electrostatic interactions was confirmed via Raman spectroscopy by comparing cys-SAM and cys-SAM-GO Raman spectra, as indicated in green and orange in Figure 3.1*a*, respectively. From Figure 3.1*a*, it can be noticed that cys-SAM-GO film displayed a typical spectrum (using a 632.8 nm excitation laser [34]), which is characterized by two predominant bands, D and G, located at approximately 1350 cm^{-1} and 1614 cm^{-1}, respectively. Typically, the G band is associated with the stretching of C-C bonds in sp^2 carbon pairs [35], and its intensity, denoted as I_G, provides information about the sp^2 domains in the carbon lattice, whereas the D band is associated with the presence of structural defects [36], corresponding to sp^3 hybridization domains that occur owing to the higher concentration of oxygenated groups. Accordingly, the intensity I_D of the D band is commonly used to estimate the

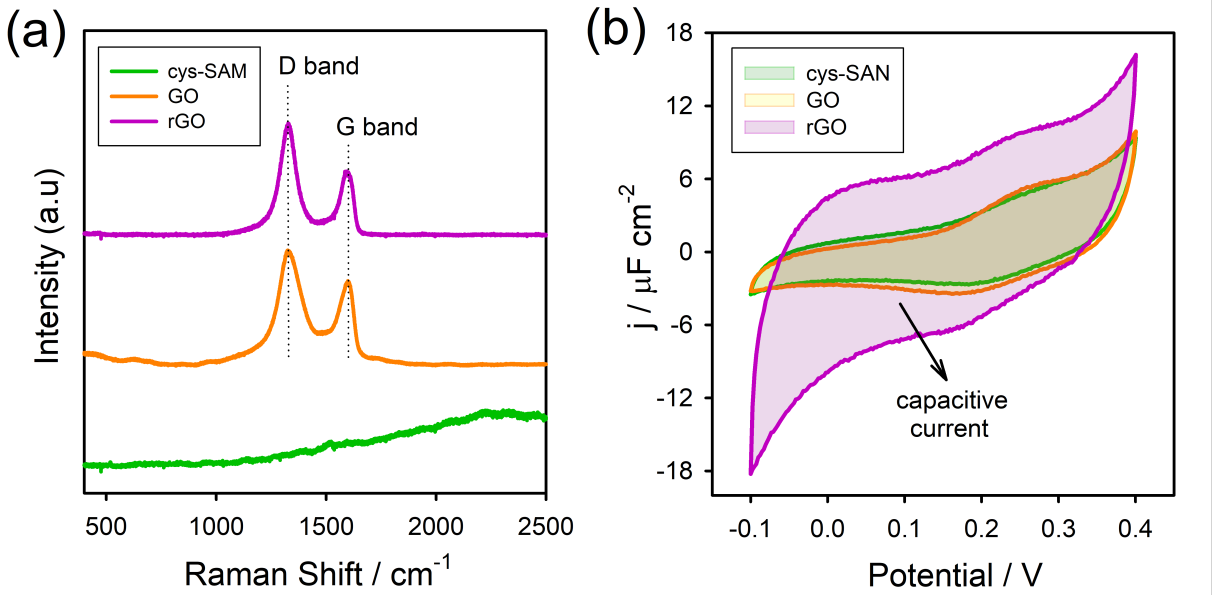

Figura 3.1: (a) Normalized Raman spectrum of cys-SAM, cys-SAM-GO (denoted simply as GO), and cys-SAM-rGO (denoted simply as rGO) structures compositions showing the D and G bands. Samples were excited by using a 638 nm laser. (b) Typical CV response of cys-SAM, cys-SAM-GO, and cys-SAM-rGO interfaces obtained at a scan rate of 0.1 V s^{-1} in a potential interval ranging from -0.1 to 0.4 V *versus* Ag|AgCl 3 mol L^{-1} in phosphate buffer used as as the electrolyte environment.

degree of structural disorder [37].

The electrochemical reduction of GO attached on Au-cys-SAM-GO interfaces is primarily identified as small shifts in the maxims of the D and G bands, specifically, from 1350 cm^{-1} to 1324 cm^{-1} and from 1614 cm^{-1} to 1588 cm^{-1}, respectively. These shifts are commonly observed in rGO obtained by the electrochemical reduction [36] of GO and were detected in the Raman spectrum.

Important for the characterization of rGO are the changes in the I_D/I_G intensity ratio [38]. The electrochemical reduction of GO to form rGO permits the elimination of oxygenated groups from the surface and edges of the structure, generating dangling bonds and atomic vacancies within the carbon lattice, leading to a disruption in the high symmetry of the hexagonal atomic lattice. Presently, the I_D/I_G was measured as 2.18 $\pm$ 0.08 for Au-cys-SAM-GO and 4.21 $\pm$ 0.18 for the Au-cys-SAM-rGO films, which confirms the increasing in the disorder level within the carbon lattice, consistent with literature's observations for the formation of rGO.

Hence, Raman spectroscopy permits characterizing the reduction of the Au-cys-SAM-GO surface to Au-cys-SAM-rGO with the possibility of quantifying the number of defects introduced by the reduction of GO through the analysis of the I_D/I_G ratio. Nonetheless, the quantification of I_D/I_G ratio in correlation with the origin of the rGO supercapa-

citance is not established since the origin of rGO supercapacitance is attributed to the increasing in the surface area. Owing to this, the role of the defects on the supercapacitance properties of rGO is not known and frequently disregarded. There are few works addressing that the origin of the supercapacitance of rGO cannot be exclusively attributed to a large surface area and that the charging of the DOS must have an important contribution. Furthermore, it has been demonstrated that the increasing of the electroactive surface area upon the reduction of GO to rGO cannot *per se* quantitatively justify the increase observed in the capacitance [31].

The differences in the electrochemical responses of Au-cys-SAM-GO and Au-cys-SAM-rGO film structures can be evaluated by CV, as shown in Figure 3.1*b*, from which it can be observed pronounced differences in the electric current responses *versus* the potential of the electrode, from which averaged capacitance values per unit of electroactive area of these film's structures can be obtained as 39.1 $\pm$ 4.2 μF cm^{-2} and 95.5 $\pm$ 9.8 μF cm^{-2} for the Au-cys-SAM-GO and Au-cys-SAM-rGO films, respectively. Note that there are no significant differences between Au-cys-SAM and Au-cys-SAM-GO films in terms of the capacitance of these interfaces with the capacitance of Au-cys-SAM measured as 34.9 $\pm$ 3.4, slightly differing from 39.1 $\pm$ 4.2 μF cm^{-2} measured for the Au-cys-SAM-GO. The percentage difference is not higher than 12%, demonstrating an insignificant capacitance contribution of the assembling of GO to Au-cys-SAM interface. On the other hand, the reduction of the GO assembled to Au-cys-SAM film exhibited an averaged capacitance value of 95.5$\pm$ 9.8 μF cm^{-2} that corresponded to a percentage difference of 173% and is this capacitance contribution that turns the rGO structure into a supercapacitive compound [31].

Although researchers are explaining this increase in the capacitance of rGO regarding GO, considering a proportional increase in the electroactive area, up to now quantitative analyses have not been conducted. Furthermore, this increase in capacitance cannot be solely based on geometric arguments and is not sustainable, owing to being detached from an electronic structural change observed in the Raman spectroscopic analysis. Additionally, the QR theory predicts the superposition of electrostatic e^2/C_e and chemical/quantum e^2/C_q states, owing to the electric-field screening of the electronic charges by the electrolyte.

This superimposed energy phenomenon is measurable as $e^2/C_\mu \sim g_e e^2/C_q$, where $g_e = 2$ is the energy degeneracy associated with the superposition of the classical and quantum states. Therefore, in agreement with the predictions of the QR theory, the geometric and electronic states are intertwined, allowing the capacitance phenomenon to be studied quantitatively by measuring the $C_q \propto$ DOS within the interface. In other words, the observed pseudocapacitive phenomena are owing to the occupancy of the DOS.

The occupancy of DOS states of rGO is the phenomenon that permits the supercapacitance of rGO compounds and has been previously suggested [31, 39, 40], but detached from a QR theoretical viewpoint. Nonetheless, the meaning of C_q associated with a significant pseudocapacitance contribution in the interface owing to the occupancy of e^2/C_q states of electroactive chemical compounds assembled over electrodes has been demonstrated. For instance, observe the case of redox-active monolayers [41, 18, 24, 21] and

Prussian blue compounds [42] that have been studied previously.

Before start analyzing the phenomenon from a QR viewpoint, note that although CV methodology can characterize the observed increase in the capacitance, it is limited in providing physical insights on the mechanisms governing rGO's supercapacitance. Owing to the nature of the quantum electrodynamics that follows $E = h\nu = e^2/C_q$ phenomenology, a time-dependent analysis is required to quantify the magnitude of the capacitance and the charging electrodynamics, which requires measuring a particular resistance quantum directly associated with the quantum capacitance of the interface. For this, time-dependent electric spectroscopic methodology is the suitable approach because it permits the evaluation of the complex capacitance of the interface, in agreement with Eq. 1.2.

Accordingly, the comparative time-dependent spectroscopic analysis of GO and rGO structures will permit us to confirm the premises of the QR theory for the supercapacitance phenomenon within rGO compounds, enlightening and demonstrating the quantum mechanical origin of the supercapacitance phenomenon observed in rGO compounds.

3.2 The Pseudocapacitance of rGO Structures

The pseudocapacitance nature of rGO is investigated in the following sections using time-dependent spectroscopic analysis in which it is confirmed that the complex capacitive response of the Au-cys-SAM-rGO interface exhibited predicted semicircle-shaped features that quantitatively follow a series RC circuit dynamics. The measurements were conducted at the open circuit potential (OCP) of the interfaces, as shown in Figure 3.2*a*.

Following series RC circuit dynamics, the capacitance values are measured at the lower frequency regime ($\omega \to 0$) of each RC process, corresponding to the real component C' of $C^*(\omega)$ measured in the lowest value of the semicircle, where the imaginary component C'' tends to null [16]. These values can be roughly estimated graphically (and more precisely by an equivalent circuit analysis) by measuring the diameter of the semicircle. Considering measurements conducted at three independent interfaces, an average capacitance value of approximately 17.8 $\pm$ 0.41 μF cm^{-2} was measured for Au-cys-SAM films compared to Au-cys-SAM-GO films , where the average capacitance value was 18.1 $\pm$ 0.6 μF cm^{-2}. These measurements demonstrate the negligible contribution of GO in increasing the capacitance of the Au-cys-SAM interface, in agreement with the CV analysis discussed previously. This negligible contribution of GO to the capacitance of the interface was also observed by others [43] and has been attributed to the insulating dielectric characteristics of the GO compounds owing to the presence of a higher concentration of oxygenated groups.

The electrochemical reduction of the GO component at the Au-cys-SAM-GO interface, resulting in a significant increase in capacitance, is confirmed by the Nyquist capacitance spectrum shown in Figure 3.2*a*. This spectrum exhibits additional semicircle-shaped contributions, indicating the presence of an additional series RC circuit component and associated relaxation dynamics. The first RC relaxation dynamics has additional capacitance contributions compared to cys-SAM-GO interface within a total capacitance

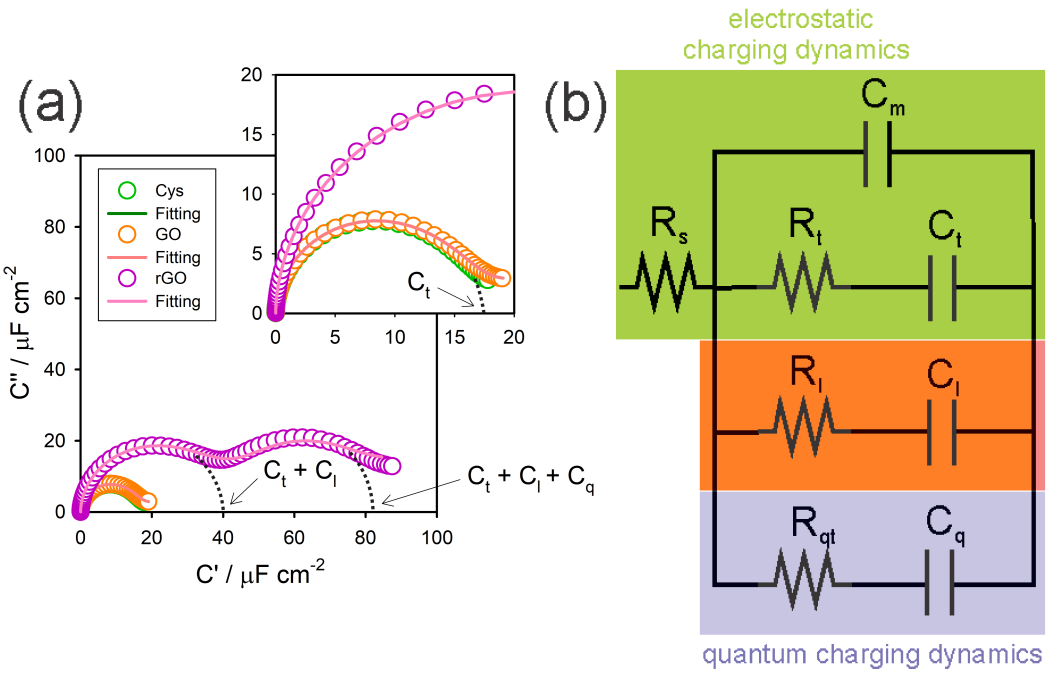

Figura 3.2: (a) Nyquist capacitive diagram obtained as described in the experimental section, in agreement with Eq. 1.2, from where the quantum capacitance and quantum RC dynamics of rGO compounds can be obtained and studied in detail. Note that the capacitance spectra of the Au-cys-SAM interface are indicated as Cys whereas the Au-cys-SAM-GO and Au-cys-SAM-rGO are denoted, respectively, as GO and rGO. Note that the addition of GO to the Au-cys-SAM interface to form the Au-cys-SAM-GO film has a negligible contribution to the total capacitance. On the other hand, upon the reduction of GO to rGO there are additional capacitive contributions. (b) Corresponds to the equivalent circuit of the interface, where the circuit within the green box indicates the electrostatic charging contribution of Au-cys-SAM and Au-cys-SAM-GO interfaces, whereas the series RC relaxations within red and purple boxes are additional contributions owing to the reduction of GO to rGO in the interface.

of $\sim$ 39.9 $\pm$ 0.75 μF cm^{-2} whereas the second RC relaxation comprises a capacitance (noted by the diameter of the second semicircle) of 40.4 $\pm$ 3.1 μF cm^{-2}. The total capacitance of about 80 μF cm^{-2} (as noted in the Nyquist plot) contribution corresponds to a percentage increase of about 370% concerning capacitance (of about 17 μF cm^{-2}) of Au-cys-SAM/Au-cys-SAM-GO interface. It is difficult to interpret this increase by solely considering an increase of the electroactive surface area owing to the electrochemical reduction of the GO component of the interface [2, 44].

These experimental results and the observed trends are in agreement with impedance spectroscopy analyses conducted by other authors [45, 46] where the capacitance obtained at higher frequencies, here associated with the increasing of the total capacitance of the first semicircle, with a capacitance of $\sim$ 39.9 μF cm^{-2}, was attributed, by others authors, to the charging of oxidized sp^2 states, whereas the increment in the capacitance

at lower frequencies, here represented by the contribution of the second semicircle, with a capacitance of $\sim 40.4\ \mu$F cm^{-2}, was attributed to the formation of point and linear defects within the basal plane and edges of the rGO structure, associated with the removal of oxygenated groups upon the reduction of GO.

Note that each capacitive semicircle shown in Figure 3.2*a* can be associated with a characteristic RC time constant $\tau_c = RC$ corresponding to a characteristic frequency of $\omega_c = 2\pi/\tau_c$, as illustrated in the capacitive Bode diagram of the Au-cys-SAM-GO and Au-cys-SAM-GO films shown in Figure S1 of the SI document.

In the next section, each characteristic RC timescale (depicted in Figure 3.2*a*) will be evaluated using a quantum RC circuit analysis combined with the QRS approach, permitting us to remove the dielectric background signal contribution of the Au-cys-SAM-GO interface from the Au-cys-SAM-rGO response. This allows us to access the quantum RC dynamics separated from existing dielectric background parasitic signals.

3.3 Traditional Equivalent Circuit Analysis of rGO Supercapacitive Films

A traditional equivalent circuit analysis of the electric response of the interface is performed in this section. The analysis considers different RC electric relaxations of the interface, i.e. those associated with the Au-cys-SAM-GO and Au-cys-SAM-rGO. Accordingly, the equivalent circuit analysis incorporates circuit relaxation processes that account for the background dielectric relaxation associated with the non-faradaic response of the Au-cys-SAM-GO interface separated from the Au-cys-SAM-rGO pseudocapacitive (quantum RC) relaxation responses.

The different series RC relaxations are noted in different colors in Figure 3.2*b*, which depicts the equivalent circuit of the interface considering the series R_s component comprising the solution/electrolyte and Au-cys contact resistances. The high-frequency static capacitance of the film (dominated by the dipolar relaxation response of the Au-cys-SAM) is represented by C_m, which is quite small compared with C_t and other capacitances of the circuit. C_m is settled in paralell to a series R_tC_t circuit that represents the low-frequency dipolar relaxation of Au-cys-SAM film [47, 48]. Parallel to R_tC_t, there is an additional series of resistive-capacitive relaxation termed R_lC_l that accounts for the high-frequency (first semicircle relaxation) quantum contribution associated with the charging of the pseudocapacitive states of the rGO component of Au-cys-SAM-rGO interface after the reduction of GO. Finally, the low-frequency charging contribution of pseudocapacitance of the Au-cys-SAM-rGO is represented, in Figure 3.2*b*, as $R_{qt}C_q$, which is also arranged in parallel to R_tC_t and R_lC_l time constants.

Note, as shown in Figure 3.2*a*, that the fit of the Nyquist capacitive spectrum to this equivalent circuit yielded a well-adjusted result with a confidence level of 99%. The averaged values of each circuit element, from the analysis of three different Au-cys-SAM-rGO films, are shown in Table 3.1. The fitting strategy consisted of initially fitting the cys-SAM spectrum separately (see ESI document for more details) aiming to estimate the

values of the circuit elements indicated in the green box of Figure 3.2*b*, which corresponds to a circuit relaxation process that models the dipolar relaxation response of a dielectric component of the cys-SAM. This procedure was better discussed in previous works [48, 47].

As the values of Au-cys-SAM-GO were not significantly different from that of Au-cys-SAM[1], the values of C_m, R_t and C_t were estimated from the fitting of Au-cys-SAM and considered as initial parameter values for the fitting of the entire equivalent circuit of the Au-cys-SAM-rGO interface, from which quantum RC characteristic time constants R_lC_l and $R_{qt}C_q$ were 'separately' evaluated. The $R_{qt}C_q$ corresponded, in agreement with the QR theory, to the measurement of the quantum rate (or to the quantum characteristic RC time constant) and consequently permitted the quantification of the quantum electrodynamics associated with charging electronic defects within the rGO chemical structure owing to the reduction of GO.

Tabela 3.1: Circuit Parameters fitted using the equivalent circuit presented in Fig.4b. $\overline{x}$ refers to the mean average value and $\sigma_{\overline{x}}$ refers to the standard error of the mean of the three independent junctions that comprises a rGO-nanofilm attached over a cysteamine monolayer

Parameter	$\overline{x}$	$\sigma_{\overline{x}}$
R_s(kΩ)	0.109	0.004
C_m (μF cm^{-2})	0.02	0.003
R_t (kΩ)	0.002	0.0001
C_t (μFcm^{-2})	17.38	0.94
R_l (kΩ)	0.063	0.013
C_l (μF cm^{-2})	22.47	2.62
R_{qt} (kΩ)	3.957	0.265
C_q (μF cm^{-2})	43.68	2.87

In other words, the capacitance spectrum recorded for Au-cys-SAM-rGO was fitted considering the contribution of Au-cys-SAM-GO separately with additional contributions comprising R_lC_l and $R_{qt}C_q$ branches added *a posteriori*, as noted, respectively, in the red and purple boxes of Figure 3.2*b*.

It is now important to comment on the meaning of the series resistance to the analysis of the relaxation processes in the traditional circuit analysis. The resistance quantum $R_q \propto h/e^2$, as demonstrated in previous works, is given by the limit of the total series resistance of the interface, i.e. $R_q = R_s + R_{q_\alpha}$, where R_α corresponds to the quantum resistance (R_l or R_q) of each RC circuit branch considered in series to the R_s. Therefore, by computing the total series resistance R_q of each RC circuit branch, in which $\omega\tau$ is the governing dynamics, the resonance process implies that $\omega\tau = 1$ and $f = 1/2\pi\tau$ (owing to $\omega = 2\pi f$), from which a characteristic $\tau = 2\pi R_qC_q$ can be obtained associated with each RC time constant, as indicated in Figure 3.2*b*, permitting to evaluate separately each relaxation process of the interface.

[1]The capacitive contribution of GO added to Au-cys-SAM is negligible, as demonstrated in the SI document.

Accordingly, for each RC time constant, considering the effect of the series resistance R_s, the $R_q = R_s + R_\alpha$ can be evaluated. By calculating the R_q associated with the branch enclosed in the red box, corresponding to τ_1, an average value of $R_q = 2\pi(R_s + R_l) = 0.172 \pm 0.024$ kΩ is obtained, which is different of the quantum limits of ~ 12.9 kΩ (regarding electron spin dynamics, as as proposed by Landauer [49]) or ~ 25.8 kΩ (disregarding electron spin dynamics, thus a value referred to R_K and known as the von Klitzing constant [50]).

On the other hand, by analyzing the electric relaxation comprising the RC time constant depicted in the purple box of Figure 3.2*b*, associated with the lower frequency response of the Nyquist capacitive spectrum of Figure 3.2*a*, a $R_q = 2\pi(R_s + R_{qt_2}) \sim 25.57$ kΩ is obtained, corresponding to the von Klitzing constant R_K within 1% of error, which is in agreement with the QR theory.

In summary, the traditional equivalent circuit analysis conducted in this section demonstrates that the charging process of rGO compounds follows quantum RC dynamics at the lower frequency limit of the complex capacitance spectrum, confirming that the capacitance nature associated with the reduction process of GO is a pseudocapacitance with a quantum mechanical characteristics that correlates with the DOS within a charging dynamics controlled by C_q.

In the following section, it will be investigated the RC relaxations present in the rGO separately from the RC relaxation of Au-cys-SAM-GO interface. This will be conducted by employing a spectroscopic subtraction of RC relaxation of Au-cys-SAM-GO interface from that of Au-cys-SAM-rGO, in which theoretically only rGO relaxations would remain. By employing this procedure, astonishingly, it will be demonstrated that both remaining relaxations of rGO incorporate only quantum mechanical relaxation contributions, demonstrating that reduction of GO to rGO permits the creation of quantum mechanical states that upon time-dependent perturbations follow quantum RC dynamics predicted by the QR theory.

3.4 Quantum Rate Spectroscopic Analysis of the rGO

To confirm that the electrodynamics required for charging rGO supercapacitive states follows the QR model within quantum electrodynamics that is responsible for the observed increase of the capacitance upon the reduction of the GO component of the interface, the capacitance spectrum of the Au-cys-SAM-rGO interface was analyzed in this section analyzed using QR spectroscopic principles. This corresponds to the use of the response of the Au-cys-SAM-GO interface as a background signal that can be subtracted from the total Au-cys-SAM-rGO spectral response of the interface.

The subtracted Nyquist and Bode spectra are shown comparatively to the entire response in Figure 3.3. As can be seen, the resulting subtracted response that corresponded to the sole response of the rGO compound can be fitted to the Eq. 1.2 (see more details in the SI document), clearly demonstrating that the electrodynamics for charging the

supercapacitive states follows the QR theory. Although this was confirmed in the last section, where it was demonstrated that the pseudocapacitive nature of the capacitance associated with the lower-frequency quantum RC relaxation process is related with charging the DOS owing to the nature of C_q that is directly proportional to the DOS, the RC analysis of the higher-frequency process was not resolved as having a quantum mechanical nature.

The spectroscopic analysis depicted in Figure 3.3*a* enabled us to obtain solely the quantum mechanical energy state contributions of the Au-cys-SAM-rGO interface separated from the dielectric parasitic contribution of the Au-cys-SAM-GO interface, with the latter being employed as a background signal that was spectroscopically removed. After the spectroscopic subtraction, it is evidenced that the classical dielectric RC response of Au-cys-SAM-GO was interfering with and preventing the nature of the quantum RC relaxation at the higher-frequency region of the capacitive spectrum to be detailed and analyzed. The successful spectroscopic subtraction of this parasitic signal from the total RC response of the Au-cys-SAM-rGO interface crystal-clearly revealed that the reduction of GO is associated with measurable and chargeable quantum mechanical energy states, as will be demonstrated as follows, demonstrating the limitations of using a traditional equivalent circuit analysis (as conducted in the previous section) to study quantum RC contributions at higher frequencies owing to the reduction of GO to rGO.

Note that the spectroscopic analysis conducted in this section is similar to that performed in redox-active Azurin protein films [41], where the redox-active quantum capacitance of the interface was subtracted from the non-faradaic response. This analysis and the meaning of the non-faradaic RC relaxation process were reviewed in reference [51] and will not be discussed here.

Nonetheless, which is important to be noted is the certainty of the equivalent circuit that predicted parallel RC series relaxations and it was solely owing to this certainty that the effective spectroscopic subtraction of the Au-cys-SAM-GO dielectric contribution from the total Au-cys-SAM-rGO response was successfully conducted. The remaining RC relaxation processes comprising two quantum RC relaxations (see Figure 3.4), constitute the response of the quantum mechanical states associated with two electronic defects within the rGO structure that can now be analyzed spectroscopically in detail. Each of these quantum RC responses corresponds to two quantum rate states ν_1 and ν_2, identified in Figure 3.3*a* at $\sim$ 380 and 13 Hz, respectively.

It is possible to assign these two quantum RC relaxations processes, corresponding to two energy states $E_1 = e^2/C_{q,1}$ and $E_2 = e^2/C_{q,2}$ within $\nu_1 \propto e^2/hC_{q,1}$ and $\nu_2 \propto e^2/hC_{q,2}$, respectively, accessible rates attributed to two types of electronic defects within the rGO electronic structure, as theoretically identified in the works reported in the literature [52, 53, 45], corresponding to two electronic induced defects owing to the reduction of the GO to rGO, in which one of these is a linear-type defect (E_1) within the edges of the rGO sheets and the other (E_2) is a point-type structural defect within the basal plane.

The assignment of these structural defects associated with the electronic type of defects observed by the QR spectroscopic analysis requires more studies either experimental or theoretical to confirm to which structural defect they are correlated. However, it is im-

portant to note that E_2 contributes at lower frequencies, producing a higher contribution to the total capacitance upon the electrochemical reduction of GO.

Following the main purpose of the present work, it is now possible to definitively prove that both E_1 and E_2 energy states have a quantum mechanical nature, which can be demonstrated by investigating the supercapacitance nature of the rGO associated with the resistance to charging the identified quantum states. Similarly to pseudocapacitance measured in redox-active monolayers within a quantum mechanical nature associated with a measurable C_q [51] the resistance to charge these states must be an integer number of the resistance quantum h/e^2. As shown in Figure 3.3, both Bode (Figure 3.3a) and Nyquist (Figure 3.3*b*) diagrams can be suitably fitted to Eq. 1.2, from which a C_{q_1} and C_{q_2} are obtained with $\nu_1 = e^2/hC_{q_1} = 1/R_qC_{q_1}$ and $\nu_2 = e^2/hC_{q_2} = 1/R_qC_{q_2}$ characteristic frequencies. The proof of this nature can thus be conducted by fitting the subtracted capacitance spectrum to Eq. 1.2, considering two relaxation processes with τ_1 and τ_2 (see section S2 in SI document for more details), from where $R_{q_1} \propto e^2/h$ and $R_{q_2} \propto e^2/h$ must be obeyed within the QR theory.

For instance, to calculate the resistance R_{q_2} associated with the relaxation process at lower frequencies from the fitting with Eq.1.2, the values of characteristic time $\tau_2 = 0.0105$ s and not-normalized capacitance $C_{q2} = 2.55$ μF ($A_e = 0.058$ cm^2), as presented in Table S1, were utilized. In this case, the calculation was conducted using the expression $R_{q_2} = 2\pi\tau_2/C_{q_2}$, which was derived from term $\omega\tau = 1$ in Eq.1.2, where the ω characteristic angular frequency is given by $\omega = 2\pi\nu$. Hence, the values, obtained from this fitting (see SI document), are confirmed to be $R_q = 2\pi\tau/C_q = e^2/h \sim 25.8$ kΩ, corresponding to the von Klitzing constant R_K [50] in both higher and lower frequency RC dynamics and hence confirming that the charging dynamics of the E_1 and E_2 energy states of rGO obeys quantum electrodynamics phenomenology within the QR theory, following a quantum RC dynamics. This confirms that the classical premises that explain the supercapacitance of graphene based solely on the contribution of the electroactive area is *per se* not sustainable.

The changes of the capacitance spectrum upon the reduction of GO to rGO are hence undoubtedly associated with the reduction process of the GO, as also reported by others [52, 43], which from a chemical viewpoint can be attributed to the restoration of sp^2 carbon domains associated with the removal of oxygenated groups upon the reduction of GO [52] with the occupancy of electronic states, leading to a mixed-valence within the carbonaceous structure of the rGO. This recovery of sp^2 carbon domains from sp^3 involves the electronic occupation of certain energy $E_{q_1} = e^2/C_{q_1}$ and $E_{q_2} = e^2/C_{q_2}$ states that are observed here as quantum RC relaxations, in agreement with the QR theory. The QR theory and this type of quantum RC dynamics do not apply only to rGO but were also previously observed in redox-active monolayers [17], molecular electronics [54, 55] driven in electrolyte environment and single-layer graphene [15].

Finally, observe that such as in the case of single-layer graphene [15] and the molecular electronics of organic semiconducting (heterocyclic) molecules [54], the electronic coupling of rGO pseudocapacitive states to the probe electrode is adiabatic (corresponding to setting $\sum_{n=1}^{N} T_n(\mu) = 1$, i.e. the transmittance of the electron as a wave is not

attenuated), in contrast with the non-adiabatic coupling of diffusionless electrochemical reaction [17], which is essentially driven by an electron tunneling term of the type $\sum_{n=1}^{N} T_n(\mu) = \exp(-\beta L)$ [17], in which β is the term that accounts for the nature of the potential barrier height of tunneling process and L for the length of the barrier in diffusionless redox reaction dynamics.

In summary, the analysis conducted in this work demonstrates that the phenomenon governing the supercapacitance properties of rGO is not exclusively associated with an increase in the electroactive surface area of rGO, but it is a result of the superposition of the electrostatic and quantum mechanical states within an electrochemical interface that is majorly pseudocapacitive in nature owing to be associated with the occupancy of electronic states of a structurally defective (mixed valence) DOS of the rGO. Because of the energy degeneracy existing between classical e^2/C_e (electrostatic) and quantum e^2/C_q capacitive states of the interface, the dominant equivalent electrochemical capacitance state of the interface e^2/C_μ is accessible and quantitatively equivalent to e^2/C_q, allowing us to directly measure a quantum electrodynamics phenomenon governing the charging process of the interface.

3.5 3D SUPERCAPACITORS ELECTRODES CHARACTERIZATION

The principal methodologies utilized for characterizing the performance of supercapacitor devices encompass galvanostatic charge/discharge (GCD), and electrochemical impedance spectroscopy (EIS). Fundamentally, these techniques facilitate the derivation of essential parameters, including the potential window (operational potential), total equivalent series resistance (ESR), and capacitance. Additional characteristics, such as specific capacitance, energy density, and power density, can be deduced from these fundamental parameters. In our configuration systems, the outcomes of GCD experiments are presented in Table 3.2, where parameters involving a potential range of 1.7 V and a fixed current density of 1.0 A g^{-1} were applied. Specific capacitance values were achieved, significantly surpassing literature-reported values of around 70 F$/g^{-1}$ at the same current range for activated carbon-activated electrodes, same here in our study. When we compare the results of $rGO-PPD//rGO-PPD_{symmetric}$ and $CoHCF-rGO//rGO-PPD_{assymmetric}$ both have superior specific capacitance then activated carbon configuration, 120 and 160 g^{-1}, respectively. Another key aspect was the results was the excellent cycling stability after 10,000 cycles, with 96 % for $rGO-PPD//rGO-PPD_{symmetric}$ while 94 % in $CoHCF-rGO//rGO-PPD_{assymmetric}$. When evaluated the power density, the rGO-PPD symetric composition demonstrated the highest value, 19.35 Wh / kg^{-1} . Our initial findings hold significant promise and are expected to contribute substantially by addressing uncertainties and discrepancies in current literature, with the potential for impactful publications. Notably, our fundamental study has garnered attention from Empresa Brasileira de Aeronáutica S/A (EMBRAER), a civil aviation company, expressing interest in our 3D symmetric supercapacitor devices utilizing modified graphene materials. The

positive outcomes observed in our results have heightened anticipation for the practical applications of this research.

Tabela 3.2: Performance results derived from galvanostatic cycling for various supercapacitor configurations at Potential range of 1.7 V and 1.0 A/g^{-1} current density. Retention after 10,000 cycles.

Dispositive device configuration	Specific capacitance (Fg($^{-1}$)	Energy density (Wh kg^{-1})	power density (W kg^{-1})	Retention (%)
Activated Carbon (AC)//Activated Carbon (AC)$_{symmetric}$	64.4	6.7	12.20	80
rGO-PPD//rGO-PPD$_{symmetric}$	120	9.4	19.35	96
CoHCF-rGO//rGO-PPD$_{assymmetric}$	160	9.4	12.35	94

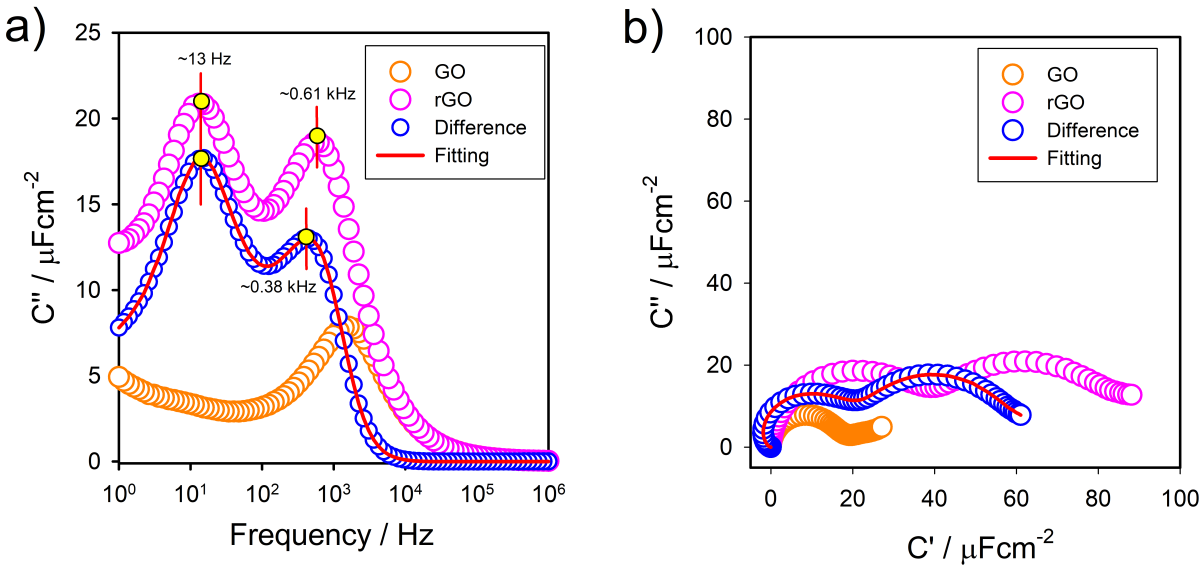

Figura 3.3: QR spectroscopic analysis of Au-cys-SAM-GO and Au-cys-SAM-rGO interfaces. (a) Imaginary Bode capacitance spectra are shown Au-cys-SAM-GO (denoted simply as GO) and Au-cys-SAM-rGO (denoted as rGO) interfaces. The capacitance spectra difference, blue circles, correspond to the subtraction of the Au-cys-SAM-GO spectrum to the total capacitance spectrum of the Au-cys-SAM-rGO interface. The procedure corresponds to the use of the spectrum response of Au-cys-SAM-GO interface as a background signal. The fitting indicated in the red curve corresponds to the adjustment of the remaining spectrum to two quantum RC circuit relaxations, in agreement with Eq. 1.2. As can be noted, the subtraction does not affect the characteristic relaxation frequencies related to the contribution of the electronic structure of rGO owing to the electrochemical reduction of GO. (b) Comparisons of the Nyquist capacitive plots of Au-cys-SAM-GO, Au-cys-SAM-rGO with the resulted spectrum (blue curve) obtained from the subtraction of Au-cys-SAM-GO to the Au-cys-SAM-rGO total response of the interface. Note that the fitting to two parallel quantum RC circuits, following Eq. 1.2 (see SI document for more details), leads to an excellent statistical agreement with $R^2 = 0.999$ in which, in both quantum RC circuit relaxation times, there was an associated (measurable) quantum resistance of $h/e^2 \sim 25.8$ kΩ.

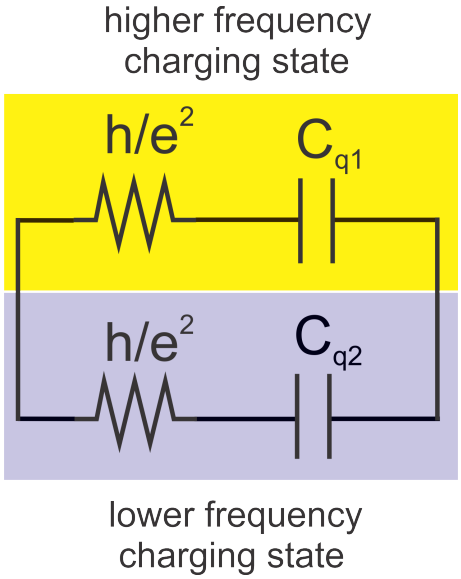

Figura 3.4: Parallel quantum RC circuit dynamics describing the two quantum RC relaxation processes experimentally observed and associated with the quantum mechanical states of the rGO electronic/structural defects. Note that this equivalent quantum RC circuit fits quite well (see SI document for more details) the subtracted complex capacitance spectroscopic response shown as the difference (blue circles) in Figure 3.3*b*. Each of these quantum RC dynamics corresponds to a type of electronic defect within of rGO's electronic structure that is experimentally accessible by the QRS, as demonstrated here.

4 Conclusions

In summary, the investigation focused on nanoscale junctions formed by rGO-nanofilms, electronically coupled to conducting electrodes via molecular bridges. The study employed Quantum Rate Spectroscopy (QRS) methodology based on impedance measurements in an electrolytic medium. The supercapacitance exhibited by rGO was attributed to a pseudocapacitive phenomenon resulting from defects induced by the electrochemical reduction of GO structures. These defects were associated with point and linear defects in the graphene structure. The capacitance spectrum revealed two relaxation processes, indicating the modification of the electronic structure by reducing GO.

Additionally, the study uncovered relativistic quantum dynamics in the electron communication between electrode and rGO nanofilm states. The electron DOS function of rGO-nanofilms was resolved through C_q response, showing agreement with DFT-calculated DOS profiles. QRS not only probes electrodynamics but also characterizes electronic structures in mild experimental conditions. The analysis of G-response demonstrated the QRS methodology's ability to access quantum insights, revealing an additional quantum degeneracy ($g_m = 3$) associated with distinct electron transport modes in rGO nanofilms.

Transitioning to energy storage, the use of 3D supercapacitors-based rGO-PPD composites as potential alternatives to lithium encountered interest. Symmetric and hybrid supercapacitors with high energy and power densities were developed, emphasizing the importance of reproducibility and electrode mass compatibility for future advancements. Despite ongoing analysis, some experimental results are still under discussion, requiring additional time for a thorough examination and theoretical analysis. This research provides a novel approach to understanding and interpreting quantum phenomena in graphene-derived structures, offering insights into the design of high-performance energy storage devices.

5 Complementar Activities

5.1 Evaluation of institutional support received in the period

The support provided by São Paulo State University "Júlio de Mesquita Filho"and the São Paulo State Research Support Foundation has been crucial for the successful execution of this project. The assistance in terms of professionals, physical space, and infrastructure for maintaining research laboratories, generously provided by Unesp and the Chemistry Institute (IQ-Araraquara), has played a pivotal role in advancing the project. Additionally, IQ-Araraquara has graciously granted access to its multi-user laboratories, which are equipped with a Raman spectrometer and other essential resources.

Financial support from the São Paulo Research Foundation, including the provision of a postdoctoral scholarship and technical reserve, has been instrumental in creating favorable conditions for carrying out the activities outlined in the projects funded by FAPESP. This combined support has been essential in ensuring the successful implementation and progress of our research endeavors.

5.2 Participation in scientific event

1- XXXIV Congresso de Iniciação Científica da Unesp-IQ/Araraquara. 29th of September 2022. (see attachment 1)

2- XXXV Congresso de Iniciação Científica da Unesp-IQ/Araraquara. 29th of September 2023. (see attachment 2);

5.3 Complementar formation

1 - Course: DESVENDANDO TECNOLOGIAS DA ELETRIFICAÇÃO DOS TRANSPORTES POR GERAÇÃO EMBARCADA. Escola de Extensão da Universidade Estadual de Campinas. 15/04/2023 to 30/04/2023, 16 total hours. (see attachment 3);

5.4 Submitted Papers

1 - Thamyres F. M. Moreira, Edgar F. Pinzón, Adriano dos Santos, Laís C. Lopes and Paulo R. Bueno. *The Quantum Mechanical Origin of the Supercapacitance Phenomenon in Reduced Graphene Oxide Structures*

5.5 Papers finalizing write and revision

1 - Thamyres F. M. Moreira, Edgar F. Pinzón, and Paulo R. Bueno. *Understanding the rGO electronic density using a spectroscopic tool*
2 - Thamyres F. M. Moreira, Edgar F. Pinzón, and Paulo R. Bueno. *Enhancing the Electronic Characterization of Graphene Quantum Dots by Quantum Rate Spectroscopy*
3 - Luiz R. Matheus, Adriano dos Santos, Thamyres F. M.Moreira, Thiago Dias, and Paulo R. Bueno. *Electroactive Electrolytes: A Breakthrough in Supercapacitor Development for Sustainable Energy Storage*
4 - Francis D. R. Garcia, Edgar F. Pinzón, Thamyres F. M.Moreira, Paulo R. Bueno. *Electrochemical and Electronic Characterization of Perovskite-Like Composites from Quantum Rate Spectroscopy*
5- Adriano dos Santos, Thiago Dias,Thamyres F. M.Moreira, and Paulo R. Bueno *Design and Characterization of a Cobalt-Based Complex for Enhanced Performance in Asymmetric Supercapacitors*

6 ATTACHMENTS

6.1 PARTICIPATION IN SCIENTIFIC EVENTS

Figura 6.1: XXXIV Congresso de Iniciação Científica da Unesp-IQ/Araraquara. 29th of September 2022. (see attachment

Figura 6.2: XXXV Congresso de Iniciação Científica da Unesp-IQ/Araraquara. 29th of September 2022. (see attachment)

7 COMPLEMENTAR FORMATION

UNICAMP

Universidade Estadual de Campinas

A Escola de Extensão da Universidade Estadual de Campinas **declara** para os devidos fins que

THAMYRES FERNANDES MESSA MOREIRA

brasileira, natural do Estado do Espírito Santo, nascida a 22 de Julho de 1990, RG: 2310559-ES, concluiu o curso de Difusão

DESVENDANDO TECNOLOGIAS DA ELETRIFICAÇÃO DOS TRANSPORTES POR GERAÇÃO EMBARCADA

ministrado pela Faculdade de Engenharia Elétrica e Computação, no período de 15/04/2023 a 30/04/2023, com carga horária total de 16 horas aula, tendo cumprido a frequência mínima para aprovação no curso.

Cidade Universitária "Zeferino Vaz", 27 de Novembro de 2023.

Professor Doutor Guilherme José de Castilho
Coordenador da Escola de Extensão

Figura 7.1: DESVENDANDO TECNOLOGIAS DA ELETRIFICAÇÃO DOS TRANSPORTES POR GERAÇÃO EMBARCADA. Escola de Extensão da Universidade Estadual de Campinas. 15/04/2023 to 30/04/2023, 16 total hours

Bibliografia

[1] SHARMA, P.; KUMAR, V. Current technology of supercapacitors: a review. *Journal of Electronic Materials*, Springer, v. 49, n. 6, p. 3520–3532, 2020.

[2] ZHAO, B. et al. Supercapacitor performances of thermally reduced graphene oxide. *Journal of power sources*, Elsevier, v. 198, p. 423–427, 2012.

[3] ARICO, A. S. et al. Nanostructured materials for advanced energy conversion and storage devices. *Nature materials*, Nature Publishing Group UK London, v. 4, n. 5, p. 366–377, 2005.

[4] MERLET, C. et al. On the molecular origin of supercapacitance in nanoporous carbon electrodes. *Nature materials*, Nature Publishing Group UK London, v. 11, n. 4, p. 306–310, 2012.

[5] HAO, L.; LI, X.; ZHI, L. *Carbonaceous electrode materials for supercapacitors*. [S.l.]: Wiley Online Library, 2013.

[6] ZHONG, C. et al. A review of electrolyte materials and compositions for electrochemical supercapacitors. *Chemical Society Reviews*, Royal Society of Chemistry, v. 44, n. 21, p. 7484–7539, 2015.

[7] MUELLER, D. N. et al. Redox activity of surface oxygen anions in oxygen-deficient perovskite oxides during electrochemical reactions. *Nature communications*, Nature Publishing Group UK London, v. 6, n. 1, p. 6097, 2015.

[8] SALANNE, M. et al. Efficient storage mechanisms for building better supercapacitors. *Nature Energy*, Nature Publishing Group, v. 1, n. 6, p. 1–10, 2016.

[9] BI, S. et al. Molecular understanding of charge storage and charging dynamics in supercapacitors with mof electrodes and ionic liquid electrolytes. *Nature Materials*, Nature Publishing Group UK London, v. 19, n. 5, p. 552–558, 2020.

[10] CHOI, J. H. et al. Graphene-based gas sensors with high sensitivity and minimal sensor-to-sensor variation. *ACS Applied Nano Materials*, v. 3, n. 3, p. 2257–2265, 2020.

[11] SENTHILKUMAR, V. et al. Comparative supercapacitance performance of cuo nanostructures for energy storage device applications. *RSC advances*, Royal Society of Chemistry, v. 5, n. 26, p. 20545–20553, 2015.

[12] BOGRACHEV, D. A.; VOLFKOVICH, Y. M.; MARTEMIANOV, S. Diagnostics of supercapacitors using cyclic voltammetry: Modeling and experimental applications. *Journal of Electroanalytical Chemistry*, Elsevier, v. 935, p. 117322, 2023.

[13] PINZON, E. F.; SANTOS, A. dos; BUENO, P. R. Density of states of a nanoscale semiconductor interface as a transduction signal for sensing molecules. *ACS Applied Electronic Materials*, v. 3, n. 8, p. 3411–3417, AUG 24 2021.

[14] PINZÓN, E. F. et al. Quantum rate as a spectroscopic methodology for measuring the electronic structure of quantum dots. *Journal of Materials Chemistry C*, Royal Society of Chemistry, 2024.

[15] BUENO, P. R.; MERCADO, D. A. M. Quantum rate theory for graphene. *Journal of Physical Chemistry C*, v. 126, n. 36, p. 15374–15385, SEP 15 2022.

[16] LOPES, L. C.; SANTOS, A.; BUENO, P. R. Measuring quantum conductance and capacitance of graphene using impedance-derived capacitance spectroscopy. *Carbon*, v. 184, p. 821–827, 2021.

[17] BUENO, P. R. Quantum rate theory and electron-transfer dynamics: A theoretical and experimental approach for quantum electrochemistry. *Electrochimica Acta*, v. 466, p. 142950, 2023. ISSN 0013-4686. Disponível em: <https://www.sciencedirect.com/science/article/pii/S0013468623011258>.

[18] ALARCON, E. V. G.; SANTOS, A.; BUENO, P. R. Perspective on quantum electrochemistry. a simple method for measuring the electron transfer rate constant. *Electrochimica Acta*, v. 398, DEC 1 2021. ISSN 0013-4686.

[19] BUENO, P. R. Electron transfer and conductance quantum. *Physical Chemistry Chemical Physics*, v. 22, n. 45, p. 26109–26112, DEC 7 2020.

[20] SANCHEZ, Y. P.; SANTOS, A.; BUENO, P. R. Quantum mechanical meaning of the charge transfer resistance. *Journal of Physical Chemistry C*, v. 126, n. 6, p. 3151–3162, FEB 17 2022. ISSN 1932-7447.

[21] SANCHEZ, Y. P.; SANTOS, A.; BUENO, P. R. Quantum rate efficiency of the charge transfer mediated by quantum capacitive states. *Electrochimica Acta*, v. 434, DEC 1 2022.

[22] BUENO, P. R. Book. *The Nanoscale Electrochemistry of Molecular Contacts*. [S.l.]: Springer, 2018. (SpringerBriefs in Applied Sciences and Technology). ISBN 978-3-319-90486-3.

[23] LOPES, L. C. et al. Electrochemical measurement of the electronic structure of graphene via quantum mechanical rate spectroscopy. *Electrochimica Acta*, Elsevier, v. 480, p. 143837, 2024.

[24] BUENO, P. R.; DAVIS, J. J. Measuring quantum capacitance in energetically addressable molecular layers. *Analytical Chemistry*, v. 86, n. 3, p. 1337–1341, FEB 4 2014.

[25] RAMESHA, G. K.; SAMPATH, S. Electrochemical reduction of oriented graphene oxide films: an in situ raman spectroelectrochemical study. *The Journal of Physical Chemistry C*, v. 113, n. 19, p. 7985–7989, 2009.

[26] TRASATTI, S.; PETRII, O. Real surface area measurements in electrochemistry. *Pure and applied chemistry*, De Gruyter, v. 63, n. 5, p. 711–734, 1991.

[27] GARROTE, B. L.; SANTOS, A.; BUENO, P. R. Perspectives on and precautions for the uses of electric spectroscopic methods in label-free biosensing applications. *ACS sensors*, ACS Publications, v. 4, n. 9, p. 2216–2227, 2019.

[28] GARROTE, B. L.; SANTOS, A.; BUENO, P. R. Label-free capacitive assaying of biomarkers for molecular diagnostics. *Nature Protocols*, v. 15, n. 12, p. 3879–3893, 2020.

[29] SMITH, C.; WHITE, H. Voltammetry of molecular films containing acid/base groups. *Langmuir*, v. 9, n. 1, p. 1–3, 1993.

[30] SHON, Y.-S. et al. Spiroalkanedithiol-based sams reveal unique insight into the wettabilities and frictional properties of organic thin films. *Journal of the American Chemical Society*, v. 122, n. 31, p. 7556–7563, 2000.

[31] GUTIERREZ, F. A. et al. Mesoscopic behaviour of multi-layered graphene: the meaning of supercapacitance revisited. *Physical Chemistry Chemical Physics*, v. 19, n. 9, p. 6792–6806, 2017.

[32] GADIPELLI, S. et al. Understanding and optimizing capacitance performance in reduced graphene-oxide based supercapacitors. *Small Methods*, p. 2201557, 2023.

[33] HUANG, Z.-D. et al. Self-assembled reduced graphene oxide/carbon nanotube thin films as electrodes for supercapacitors. *Journal of Materials Chemistry*, Royal Society of Chemistry, v. 22, n. 8, p. 3591–3599, 2012.

[34] PÉREZ, L. A.; BAJALES, N.; LACCONI, G. I. Raman spectroscopy coupled with afm scan head: A versatile combination for tailoring graphene oxide/reduced graphene oxide hybrid materials. *Applied Surface Science*, Elsevier, v. 495, p. 143539, 2019.

[35] BÎRU, E. I.; IOVU, H. Graphene nanocomposites studied by raman spectroscopy. *Raman Spectrosc*, InTech, v. 9, p. 179, 2018.

[36] ECKMANN, A. et al. Probing the nature of defects in graphene by raman spectroscopy. *Nano letters*, ACS Publications, v. 12, n. 8, p. 3925–3930, 2012.

[37] CHERUKU, R.; BHASKARAM, D. S.; GOVINDARAJ, G. Variable range hopping and relaxation mechanism in graphene oxide sheets containing sp 3 hybridization induced localization. *Journal of Materials Science: Materials in Electronics*, Springer, v. 29, p. 9663–9672, 2018.

[38] EIGLER, S.; DOTZER, C.; HIRSCH, A. Visualization of defect densities in reduced graphene oxide. *Carbon*, Elsevier, v. 50, n. 10, p. 3666–3673, 2012.

[39] BUENO, P. R. Nanoscale origins of super-capacitance phenomena. *Journal of Power Sources*, v. 414, p. 420–434, FEB 28 2019.

[40] PATHAK, A. et al. Enhanced pseudocapacitance of moo3-reduced graphene oxide hybrids with insight from density functional theory investigations. *The Journal of Physical Chemistry C*, ACS Publications, v. 121, n. 35, p. 18992–19001, 2017.

[41] BUENO, P. R.; MIZZON, G.; DAVIS, J. J. Capacitance spectroscopy: A versatile approach to resolving the redox density of states and kinetics in redox-active self-assembled monolayers. *Journal of Physical Chemistry B*, v. 116, n. 30, p. 8822–8829, AUG 2 2012.

[42] OLIVEIRA, R. M.; FERNANDES, F. C.; BUENO, P. R. Pseudocapacitance phenomena and applications in biosensing devices. *Electrochimica Acta*, Elsevier, v. 306, p. 175–184, 2019.

[43] TOH, S. Y. et al. Graphene production via electrochemical reduction of graphene oxide: Synthesis and characterisation. *Chemical Engineering Journal*, Elsevier, v. 251, p. 422–434, 2014.

[44] KIM, K. H. et al. High quality reduced graphene oxide through repairing with multi-layered graphene ball nanostructures. *Scientific reports*, Nature Publishing Group UK London, v. 3, n. 1, p. 3251, 2013.

[45] CASERO, E. et al. Differentiation between graphene oxide and reduced graphene by electrochemical impedance spectroscopy (eis). *Electrochemistry Communications*, Elsevier, v. 20, p. 63–66, 2012.

[46] BONANNI, A.; PUMERA, M. High-resolution impedance spectroscopy for graphene characterization. *Electrochemistry communications*, Elsevier, v. 26, p. 52–54, 2013.

[47] GOES, M. S. et al. A dielectric model of self-assembled monolayer interfaces by capacitive spectroscopy. *Langmuir*, v. 28, n. 25, p. 9689–9699, JUN 26 2012.

[48] LEHR, J. et al. Mapping the ionic fingerprints of molecular monolayers. *Physical Chemistry Chemical Physics*, v. 19, n. 23, p. 15098–15109, JUN 21 2017. ISSN 1463-9076.

[49] LANDAUER, R. Spatial variation of currents and fields due to localized scatterers in metallic conduction. *IBM J. Res. Dev.*, v. 1, p. 223–231, 1957.

[50] KLITZING, K. von. Developments in the quantum hall effect. *Philosophical Transactions of the Royal Society A: Mathematical, Physical and Engineering Sciences*, The Royal Society London, v. 363, n. 1834, p. 2203–2219, 2005.

[51] BUENO, P. R. Quantum electromagnetic rate theory of the electron and the meaning of the fine-structure constant. 2023.

[52] FUJII, S.; ENOKI, T. Rearrangement of π-electron network and switching of edge-localized π state in reduced graphene oxide. *ACS nano*, ACS Publications, v. 7, n. 12, p. 11190–11199, 2013.

[53] BANSAL, T. et al. New insights into the density of states of graphene oxide using capacitive photocurrent spectroscopy. *Carbon*, v. 50, n. 3, p. 808–814, 2012.

[54] NIETO, E. F. P. et al. Quantum rate electrodynamics and resonant junction electronics of heterocyclic molecules. *arXiv preprint arXiv:2309.05754*, 2023.

[55] SANTOS, A. et al. Introducing mesoscopic charge transfer rates into molecular electronics. *Physical Chemistry Chemical Physics*, v. 22, n. 19, p. 10828–10832, MAY 21 2020.